



**HAL**  
open science

## Texture analysis as a tool to study the kinetics of wet agglomeration processes

Silvia Nalesso, Carlo Codemo, Erica Franceschinis, Nicola Realdon, Riccardo Artoni, Andrea Santomaso

► **To cite this version:**

Silvia Nalesso, Carlo Codemo, Erica Franceschinis, Nicola Realdon, Riccardo Artoni, et al.. Texture analysis as a tool to study the kinetics of wet agglomeration processes. *International Journal of Pharmaceutics*, 2015, 485 (1-2), pp. 61-69. 10.1016/j.ijpharm.2015.03.007 . hal-01591577

**HAL Id: hal-01591577**

**<https://hal.science/hal-01591577>**

Submitted on 21 Sep 2017

**HAL** is a multi-disciplinary open access archive for the deposit and dissemination of scientific research documents, whether they are published or not. The documents may come from teaching and research institutions in France or abroad, or from public or private research centers.

L'archive ouverte pluridisciplinaire **HAL**, est destinée au dépôt et à la diffusion de documents scientifiques de niveau recherche, publiés ou non, émanant des établissements d'enseignement et de recherche français ou étrangers, des laboratoires publics ou privés.

# 1 Texture analysis as a tool to study the kinetics of wet agglomeration processes

2 Silvia Nalesso<sup>a</sup>, Carlo Codemo<sup>b</sup>, Erica Franceschinis<sup>b</sup>, Nicola Realdon<sup>b</sup>, Riccardo Artoni<sup>c</sup>, Andrea C.

3 Santomaso<sup>a,\*</sup>

4 <sup>a</sup>APTLab - Advanced Particle Technology Laboratory, University of Padova, Department of Industrial Engineering, via

5 Marzolo 9, 35131 Padova, Italy

6 <sup>b</sup>PharmaTeG - Pharmaceutical Technology Group, University of Padova, Department of Pharmaceutical and

7 Pharmacological Sciences, via Marzolo 5, 35131 Padova, Italy

8 <sup>c</sup>LUNAM Université, IFSTTAR, site de Nantes, MAST/GPEM, Route de Bouaye CS4, 44344 Bouguenais, France

9  
10 \* corresponding author: tel. +39 049 8275491 email address: andrea.santomaso@unipd.it (Andrea C. Santomaso)

## 11 12 Abstract

13 In this work wet granulation experiments were carried out in a planetary mixer with the aim  
14 to develop a novel analytical tool based on surface texture analysis. The evolution of a simple  
15 formulation (300 g of microcrystalline cellulose with a solid binders pre-dispersed in water) was  
16 monitored from the very beginning up to the end point and information on the kinetics of  
17 granulation as well as on the effect of liquid binder amount were collected. Agreement between  
18 texture analysis and granules particle size distribution obtained by sieving analysis was always  
19 found. The method proved to be robust enough to easily monitor the process and its use for more  
20 refined analyses on the different rate processes occurring during granulation is also suggested.

21  
22 *Keywords:* wet granulation, granulation kinetics, planetary mixer, texture analysis

## 23 1. Introduction

24 Wet granulation is a common pharmaceutical operation aiming at eliminating unfavorable  
25 properties of fine powders, improving flow properties, compaction characteristics and composition  
26 homogeneity of the granulated products. It is usually performed in four phases: (1) homogenization  
27 of dry powders; (2) liquid addition; (3) wet massing with liquid feeding system switched off; (4)

28 granules drying. All these phases (excepted drying) are often carried out in mechanically agitated  
29 vessels which can promote efficient mixing also of cohesive materials. Such mixers exert an intense  
30 local shear on the powder which breaks down the small cohesive aggregates (Harnby, 1997),  
31 promotes a good liquid dispersion and a proper product consolidation (Cavinato et al., 2010). They  
32 are generally constituted by a vessel and an impeller rotating about an horizontal or a vertical axis.  
33 When rotating about a vertical axis, the impeller can also revolve following circular trajectories so  
34 that these mixer-granulators are called planetary or orbital mixers (Laurent, 2005; Hiseman et al.,  
35 2002). In some cases the rotating axis does not revolve but it is the vessel that rotates (Boerefijn et  
36 al., 2009). Despite the large use of this type of granulators in many industrial processes, the  
37 agglomeration mechanisms caused by liquid binder addition are currently not totally understood  
38 (Laurent, 2005; Knight et al., 2001). Granulation can be indeed affected by a large number of  
39 variables, including process parameters, material properties and formulation variables (Faure et al.,  
40 2001). Monitoring the behavior of a wet bed of powders and following its evolution during time is  
41 of paramount importance to design, analyze and control the pharmaceutical manufacturing process  
42 in a Process Analytical Technology (PAT) perspective. Different techniques have been used in the  
43 past to monitor and carry out a description of the powder agglomeration process within the mixer-  
44 granulator. A comprehensive review of such techniques can be found in Watano (2001). Most of the  
45 measurement methods can give an indirect information on the status of the granulation process  
46 since they do not observe the particles directly but they measure physical variables supposed to be  
47 related to particle size. Acoustic emission, for example, has shown possibilities for granulation end-  
48 point detection (Briens et al., 2007). Also amperage or motor power consumption and impeller  
49 torque are frequently monitored as indirect measures of the agglomeration process. Particularly,  
50 power consumption and impeller torque have been used to identify how the system evolve during  
51 the agglomeration as a function of mixer geometric configuration (impeller and bowl shape) and  
52 impeller speed (Paul et al., 2003). Leuenberger et al. (2009) have investigated the relationship

53 between granule growth and power consumption curves and have demonstrated the possibility of  
54 end-point determination by power consumption monitoring. Bier et al. (1979) also reported that  
55 records of power consumption and torque were in good agreement. In alternative to the end point  
56 determination Leuenberger et al. (2009), torque has been used also to predict the starting point of  
57 granulation (Cavinato et al., 2010, 2013) as a function of liquid binder amount. All this methods  
58 however, even if effective in collecting information about the process, are indirect; other techniques  
59 can give a more direct information on the status of the granules in the mixer-granulator. Techniques  
60 such as the focused beam reflectance measurement (FBRM), which allows to follow the granule  
61 chord length evolution in real time (Huang et al. 2010), are starting to be used in wet granulation  
62 studies. Also the simultaneous combination of different techniques such as FBRM, acoustic  
63 emission measurement and near infrared spectroscopy have been used to asses granulation rates in  
64 fluidized beds (Tok et al., 2008). A direct measurement and control of granule growth can be also  
65 achieved through the use of sensors capturing digital images of the powder bed and analyzing them  
66 with image analysis techniques. Image processing systems have been used for direct and continuous  
67 monitoring of the granule growth in fluidized bed granulation (Watano, 2001) and in high shear  
68 granulators (Watano et al., 2001). Since all the above techniques try to identify each particle  
69 individually, issues related to particles overlapping and contacts, and to the minimum number of  
70 particles to be analyzed exist. For process control purposes it would be advisable to develop PAT  
71 analyzers able to process thousand of particles simultaneously and extract averaged information on  
72 the status of the granular mixture during time, possibly providing real-time process information.  
73 Texture analysis (TA) of digital images of the powder bed surface (also known as surface imaging  
74 (Lakio et al., 2012)) can be potentially used in this sense. TA is already used in a variety of  
75 applications spanning from remote sensing to automated inspection and medical image processing  
76 (Russ, 1999; Gonzales et al., 2004). The basic idea behind the use of TA is that smooth surfaces will  
77 have small variation in gray scale values and the rougher the surface the larger are the variations. In

78 the pharmaceutical context it has been used to determine the particle size distribution (PSD)  
79 (Laitinen et al., 2002) and the segregation tendency of granulated products (Lakio et al., 2012) in  
80 static conditions. In this work the wet granulation process was studied with TA by taking time series  
81 of digital images of the moving powder bed inside the granulator during the whole granulation  
82 process. The subsequent analysis was therefore carried out on the bulk powder (not on single  
83 granules) and its evolution from being a dry mixture up to a wet mass of distinct aggregates was  
84 monitored and studied. The aim of the work was to assess if TA can be used as an analytical tool to  
85 observe the effect of different liquid binder addition rates and amounts on the granulation kinetics  
86 and on product properties.

87 The paper is structured as follow: in Section 2 some principles of image and texture analysis  
88 are resumed and the texture descriptors, the experimental set-up and the materials are presented.  
89 The potential of the texture analysis is verified and tested in Section 3 with preliminary experiments  
90 in simplified and controlled conditions. In Section 4 the use of TA is finally described in wet  
91 granulation experiments where the granulation kinetics are measured as a function of binder  
92 addition rate and the effects of binder total amount on granules PSDs are described.

93

## 94 **2. Experiments and methods**

### 95 ***2.1. Texture analysis***

96 The main advantages of looking at surface texture are that the technique is not invasive and  
97 the particles are not analyzed individually but in bulk. Moreover issues on sample preparation, on  
98 the number of granules to be analyzed, on the dispersion of the material to avoid particles  
99 overlapping and contacts are therefore avoided. Since the camera can be positioned far enough from  
100 the moving powder bed, fouling of the lenses can be avoided as well. This allows to analyze a  
101 moving bed of particles provided that the surface is sufficiently defined and a suitable lightning  
102 source is available.

103 TA attempts to quantify intuitive qualities described by terms such as rough, smooth, silky or  
104 bumpy as a function of the spatial variation in pixel intensities on gray-scale digital images that in  
105 our case are pictures of the powder bed surface (Laitinen et al., 2002). A digital image (raster or  
106 bitmap image) is a binary representation of a two-dimensional image with a finite set of digital  
107 values, called picture elements or pixels. Pixels are ordered in a fixed number of rows and columns  
108 and hold a set of quantized values that represent the color and the brightness at any specific point.  
109 Often for scientific and industrial purposes digital images are in gray-scale i.e. only the brightness  
110  $z_i$  (or intensity level) is given for each pixel (Russ, 1999; Gonzales et al., 2004). The index  $i$   
111 indicate the level number which for a 8 bit image spans from 0 to  $2^8 = 256$ . Level intensities can be  
112 graphically represented according to their frequency of appearance in the image (number of pixels  
113 with a given intensity) as histograms  $f(z_i)$ . Two examples of intensity histograms are shown in  
114 Figure 1. They characterize two images of generic granules with different size. It can be appreciated  
115 also by simple visual inspection that the larger the granules size, the more contrasted the surface  
116 and the broader the corresponding histogram, i.e.  $f(z_i)$  spreads over a larger number of intensity  
117 levels. It is therefore clear that a correlation between intensity level histogram, texture of the image  
118 and particle size exists and this correlation can be used to study the granulation process where  
119 changes in size of the wet aggregates occur.

120 Several texture descriptors of different complexity exist. In order of increasing complexity,  
121 we can enumerate descriptors based on the average value, the standard deviation (STD), the third  
122 moment of the intensity level histogram and those based on the gray level co-occurrence matrix  
123 (GLCM). GLCM is a second order statistics which describes the spatial correlation between couples  
124 of neighbouring pixels by compiling the frequency for which different gray level intensities are  
125 found in a defined area (Gosselin at al., 2008). On the whole 11 descriptors have been considered  
126 but finally the standard deviation STD of  $f(z_i)$  has been used in this study since most of the texture  
127 descriptors were found to be equivalent to STD (the same or similar information could be

128 extracted). Similarly to other texture descriptors (such as smoothness, uniformity or entropy which  
129 implementation can be found in Gonzales et al., 2004) STD is based on some statistics performed  
130 on  $f(z_i)$ . In particular the STD in mathematical form is expressed as:

$$131 \quad \sigma = \sqrt{\mu_2(z_i)} \quad (1)$$

132 and is related to the second moment,  $\mu_2$ , about the mean  $m$  of the histogram  $f(z_i)$ :

$$133 \quad \mu_2 = \sum_{i=0}^{L-1} (z_i - m)^2 f(z_i) \quad (2)$$

134 From the observations and reasonings made on Figure 1 it is intuitable that the STD, which  
135 is recognized as a simple but robust measure of the average contrast of the image (Gonzales et al.,  
136 2004), has the potential for being used as an analytical tool in the granulation process.

137

## 138 **2.2. Image Acquisition**

139 Two different types of experiments were performed, static and dynamic tests, with  
140 increasing level of difficulty for the image acquisition process. Static tests were performed on small  
141 samples of granulated dry materials of known particle size and size distribution, in order to verify  
142 the feasibility of the TA in simplified conditions. Tests were performed in a simple ad hoc setup  
143 with controlled lightning conditions. It was a photographic box made of an open vertical PVC  
144 cylinder (150 mm in diameter and 200 mm long); the powder was put in a 25 cm<sup>3</sup> cup (27.4 mm in  
145 diameter) placed at center of the cylinder base (Figure 2). The light source was constituted by a  
146 continuous strip of white LEDs fitted to the internal wall of the box to form a ring. A digital camera  
147 (DBK-61BUC02, 1/2" CMOS, 2048×1536, The Imaging Source, Bremen, Germany) with  
148 12mm/1:1.4 lens (Pentax) and a 5 mm spacer was aligned on the top of the cylinder axis to take  
149 pictures of the sample surface.

150 In the dynamic tests the same camera was placed above the mixer vessel but for geometric  
151 constraints due to the arm holding the impeller, it was not axially positioned. Because of the offset  
152 only a portion of the bed surface was monitored. The image acquisition process was automated at a

153 frame rate of 0.5 fps and with an exposure time of 1/714 s. A relatively short exposure time was  
154 required to avoid the blurring of the images due to the surface motion. As a consequence of the  
155 short exposure time of the CMOS sensor a more intense lighting of the surface was required. The  
156 light source was constituted by three continuous strips of white LEDs (instead of one as in the static  
157 experiments) fitted to form three rings. The rings were fixed to the mixer internal wall through a  
158 metallic structure (Figure 3). In both cases the height of the light source with respect to the powder  
159 surface was roughly 80-90 mm, while that of the camera was 290 mm.

160       Because of the orbital motion it could be that the impeller appeared in some of the images  
161 taken during the granulation experiments biasing the analysis. The upper part of the impeller was  
162 therefore painted green and pictures containing green pixels were automatically discarded by  
163 working in the HSV (hue, saturation and value) color-space where green was found in the range  
164 0.3-0.4 of the hue channel (Dal Grande et al., 2008). The image selection procedure and the TA  
165 were not performed on the full image but on a region of interest (ROI) of size 200 x 300 pixels. The  
166 resolution of the images was 105  $\mu\text{m}/\text{pixel}$ , so that the observation area was 21.0 x 31.5 mm large.  
167 The size, the shape and the position of the ROI were chosen with a trial and error procedure in order  
168 to minimize the presence of the impeller blade in the pictures and consequently the number of  
169 discarded images during the analysis. On the average 15% of the images were discarded. After  
170 selection, the ROI was converted to gray-scale and processed by TA. All the softwares for image  
171 selection and for TA were customized and written in Matlab (MATLAB 7.5 and Image Processing  
172 Toolbox 6.0, The MathWorks, Inc., Natick, Massachusetts, United States). Image acquisition  
173 instead was performed with the software bundled with the digital camera (IC Capture v2.2).

174

### 175 ***2.3. Powders and granulating liquid***

176       A simple formulation made up of microcrystalline cellulose (T1 Ph. Eur., MCC) was chosen  
177 as it is commonly used in pharmaceutical granulations and has porous particles able to absorb high

178 amount of granulation liquid. The batch size was 300g. The MCC particle size, determined with  
179 Malvern Mastersizer 2000 (Worcestershire, 185 UK), expressed as  $d_{10}$ ,  $d_{50}$ ,  $d_{90}$  resulted equal to 13,  
180 48 and 176  $\mu\text{m}$  respectively.

181 Dispersion in water of xanthan gum (XG) at 0.05w/w% was used as liquid binder. XG is a  
182 polysaccharide produced by aerobic fermentation of glucose, sucrose or lactose by the bacterium  
183 *Xanthomonas campestris*. It is used as a pharmaceutical thickening agent and as a stabilizer and  
184 thickening agent in food preparations (E415) because of its strong thickening power (Litster and  
185 Ennis, 2004). In order to obtain the liquid binders, XG powder was pre-dispersed in water. In this  
186 way complications related to additional rate processes such as the hydration of the solid binder  
187 during the granulation process were avoided.

188 The viscosity of the binder aqueous dispersion was measured with a rotational viscometer  
189 (Rotovisco RV20, Haake, Germany) and the surface tension with the sessile drop method  
190 (Middlemann, 1995). Their values were respectively 30 mPa s and 0.069 N/m, while the density  
191 was 998.0 kg/m<sup>3</sup>.

192 MCC and XG powders were provided by ACEF SpA, Fiorenzuola d'Arda, Piacenza, Italy.

193

#### 194 **2.4. Granulation procedure**

195 Experiments have been carried out in a planetary mixer (Kenwood Major Premier KMM  
196 760, Kenwood Ltd., London, UK) which consisted of a bowl 200 mm high with 230 mm maximum  
197 diameter and 6.7 l total volume. A standard K shaped impeller was used. The mixer bowl was open  
198 at the top so that it was possible to observe the powder bed by visual or camera inspection during  
199 the granulation process and a sensor was used to collect digital images of the powder bed as  
200 described in Section 2.2. The mixer was operated at constant impeller speed of 100 rpm in all the  
201 experiments. The ratio between rotations and revolutions was fixed by a gearing ratio of 3.333. The  
202 working conditions were chosen in order to ease the development of the analytical method based on

203 TA. A detailed description of this specific mixer geometry and of the flow patterns inside the mixer  
204 can be found in dedicated papers (Hiseman et al., 2002; Laurent, 2005).

205 The granulation procedure followed these steps: a) powder loading, b) dry mixing (3  
206 minutes), c) wetting phase (with variable length from 4 to 36 minutes according to liquid binder  
207 addition rate), d) massing phase (5 minutes), e) granules discharge and f) drying.

208 The liquid binder was added to the MCC using a peristaltic pump (Velp SP 311/2) by dripping from  
209 three evenly spaced points (droplet size was approximately 4 mm). The amount of liquid was fixed  
210 to 330 g excepted where specified. The feed flow rate adopted in the experiments were in the range  
211 9 to 83 ml/min. The feed rate was monitored by measuring the decrease in weight of the liquid  
212 remaining in the reservoir (see Figure 3). Granules were then dried in a ventilated oven at  
213 temperature of 50°C overnight and sieved (AS 200 control Retsch, Germany) using the following  
214 sieves: 45, 100, 200, 300, 400, 500, 600, 710, 800, 1000, 1410, 2000, 5000  $\mu\text{m}$ .

215

### 216 **3. Results and discussion**

217 Preliminary static tests (out of the mixer) and dynamic tests (within the mixer) were carried  
218 out in dry conditions in order to validate the TA and verify its ability to distinguish between powder  
219 mixtures made of particles with different sizes. This was of course a necessary prerequisite to  
220 develop an analytical method able to follow particle size variations in time as a consequence of  
221 liquid binder addition. It is important to emphasize here that no attempt were made to determine the  
222 full PSD of the granulation products with TA since this task is beyond the scopes of this work. In  
223 previous literature works full PSDs of granules have been measured with TA by using static samples  
224 under sequential bidirectional lightning (Laitinen et al., 2002; Lakio et al., 2012). The strictly  
225 controlled lighting conditions adopted in such works can not be obtained inside the mixer in  
226 dynamic conditions so that we limited the study to the use of a simple texture index, the STD,  
227 related to particle size in average sense.

### 228 **3.1. Preliminary static tests**

229 Two different tests were performed using static samples. The first test was made on  
230 monodispersed powders or granules. A granulated microcrystalline cellulose was sieved in 7 size  
231 ranges (spanning from 50 to 1000  $\mu\text{m}$ ). Images of bulk powder belonging to each size range were  
232 taken in the photographic box and surface texture was analyzed. The results in terms of STD of the  
233 gray-scale histogram are shown in Figure 4 where it can be appreciated that the STD increased  
234 monotonically with the granules size in a quite large size range. A second test was then made in  
235 order to verify if TA was effective also with polydispersed powder mixtures of smaller size (which  
236 is more similar to what can be found in a granulator especially in the early stages of the process).  
237 Different quantities of MCC particles ( $d'_{50} = 75 \mu\text{m}$ ) and granules ( $d''_{50} = 250 \mu\text{m}$ ) were mixed  
238 together in 8 different proportions (0, 0.1, 0.2, 0.4, 0.5, 0.6, 0.8, 1.0 expressed as fractions of the  
239 granules weight) and analyzed as previously described for the monodispersed case. Also in this case  
240 the TA was able to distinguish between different samples with a roughly linear trend of the STD as a  
241 function of the average particle size of the mixture calculated as  $d'_{50} w + d''_{50} (1 - w)$ , where  $w$  is the  
242 weight fraction of larger particles (Figure 5).

243

### 244 **3.2. Preliminary dynamic tests**

245 The observation of the powder bed surface in process conditions, i.e. within the mixer with  
246 impeller rotating at 100 rpm, was a more complex task than in static conditions. Many issues can  
247 indeed affect the dynamic image acquisition:

- 248 • changes of distance between the powder bed surface and the CMOS sensor which occur  
249 during the granulation process when powder is moving or when becomes wet (focusing  
250 problems);
- 251 • particles in rapid motion (causing motion blurring in some portions of the image);
- 252 • uneven surface illumination (due to the impeller position, for example, which can generate

- 253 shadows on the surface biasing texture identification);
- 254 • insufficient illumination (due to the reduced sensor exposure time, required to reduce
  - 255 motion blurring);
  - 256 • impeller presence in the visual field (hindering the powder surface observation).

257 Optimal conditions for bed surface observation were therefore found through dedicated tests  
258 performed in dynamic conditions on 7 monodispersed MCC granulated particles (sizes from 100 to  
259 3000  $\mu\text{m}$ ). The relationship between STD and particle size are reported in Figure 6. Also in this case  
260 a trend with the particle size was found. TA and in particular the use of STD demonstrated to be  
261 robust and reliable enough to follow and analyze the changes in size occurring in the planetary  
262 mixer. All the preliminary tests (static and dynamic) were successfully performed in different size  
263 ranges typical of the industrial granulation processes (from 75 to 3000  $\mu\text{m}$ ) suggesting therefore the  
264 possibility of developing an analytic tool able to follow the granulation process from the very  
265 beginning up to the end point.

266

### 267 **3.3. Results from the process**

268 The wet granulation experiments were carried out in the planetary mixer. In order to  
269 appreciate the agglomeration process Figure 7 reports some pictures of the powder surface at  
270 increasing time intervals. It is evident, even by simple visual inspection, that at minute 4 the surface  
271 becomes progressively rougher (liquid addition started at minute 3). This corresponded to an  
272 increase of the MCC particles cohesion mediated by capillary forces. The cohesion caused the  
273 particle to aggregate forming increasingly larger agglomerates, the enlargement process reached a  
274 maximum at 14 minutes and then the agglomerates started to reduce in size up to a final equilibrium  
275 value. It is interesting (and at the same time counterintuitive) to note that the size of the  
276 agglomerates started to reduce before the addition of liquid binder was stopped. Liquid addition  
277 stopped at minute 16 while the decrease in size started at minute 14 (i.e. 2 minutes before). This

278 behavior is common to all the experiments so it is important, in this context, to verify if the  
279 proposed analytical tool, based on image analysis, was able to detect it. This was done by  
280 comparing the visual information of Figure 7 with the response of the TA. In Figure 8 the STD  
281 profile of the above experiment is reported as a function of time. The start and the stop time of  
282 liquid addition are represented in Figure as vertical dashed lines.

283         An increase in STD was expected after minute 3 and indeed, after an initial dry mixing step  
284 where STD remained constant at a minimum value, a linear increase of the profile was observed  
285 after starting liquid addition. The change of surface texture (quantified by an increase of image  
286 contrast) was therefore correctly detected by the STD and could be correlated to the progressive  
287 increase in size of the MCC agglomerates observed in Figure 7. At a given time (in this case  
288 roughly at minute 12) STD reached a maximum and then started to decrease meaning that surface  
289 texture tended to homogenize because of a size reduction of the largest aggregates in the mixture.  
290 TA was therefore in complete agreement with the initial visual observation that the maximum size  
291 of the agglomerates was reached before the stopping of the liquid feeding. At the end of the process  
292 the STD profile tended to become flat meaning that an equilibrium between the different and  
293 competing agglomeration mechanisms was reached and size remained constant.

294         To assess the reliability of the method, the variability associated to the joint effects of the  
295 granulation experiments and of the TA was evaluated with replicated tests performed in the same  
296 conditions. Figure 9, shows the result of three replicated granulation tests carried out at 28 ml/min  
297 of binder flow rate. The average STD profile and the corresponding error bars (representing the  
298 standard deviation of STD at each monitored time) are reported. It can be observed that the  
299 variability of the STD was not constant during the process. It was minimum in the early stages of  
300 the process ( $\pm 6\%$ ), then increased reaching a maximum before the STD peak ( $\pm 12\%$ ) and then  
301 reduced towards the end where the profile tended to become flat ( $\pm 6\%$ ). So even if the general trend  
302 of the STD profiles is clear, it happens that while the early stages and the end point of the

303 granulation process can be characterized quite confidently by TA, attention should be paid looking  
304 at the central stage of the granulation process where STD variability is larger.

305

### 306 **3.4. Effect of binder flow rate**

307 In order to study the applicability of the TA on granulation kinetic studies experiments at  
308 different liquid binder flow rate (9, 22, 28, 47, 83 ml/min) were performed. The liquid binder was a  
309 dispersion of XG in water (0.05 w/w%).

310 Since the amount of liquid binder was fixed to 330 g so the duration of each experiment was  
311 different with the wetting phases lasting respectively 36, 15, 12, 7 and 4 minutes. Results are  
312 reported as STD profiles in Figure 10 where it is evident their strong dependence on the binder flow  
313 rate. In particular the following observations can be done:

- 314 • the overall shape of the profile did not change since they all showed a maximum of STD;
- 315 • the early stages of the process (nucleation and growth) were strongly influenced by the  
316 binder flow rate;
- 317 • the maximum of the STD (i.e. the maximum size of the wet agglomerates) was always  
318 reached before the stopping of the binder feeding (stopping time is not reported in the  
319 Figures for sake of clarity, it always occurred 5 minutes before the end of the granulation  
320 process because the massing time was a constant);
- 321 • the final level of the STD profiles (i.e. the final sizes of the wet agglomerates) were roughly  
322 constant, independent of the flow rate and of the process length;

323 A more detailed analysis can be carried out by quantifying the slope  $m$  of the profiles through two  
324 linear fittings performed before and after the maximum of STD (Figure 10: a and b respectively).

325 Kinetic information are summarized in Figure 11 where the value of the kinetic constants (slopes of  
326 the linear fitting) are reported as function of the binder flow rate. It can be observed that while the  
327 growth rates increased with the binder flow rate, the size reduction rates were almost constant and

328 independent of binder flow rate, which is consistent with the fact that the operating conditions were  
329 nearly the same in this stage of the process. This again indicates that TA response is sensitive to and  
330 coherent with the physical changes of the system. Figure 12 instead shows the liquid to solid ratio,  
331  $L/S$ , required to reach the maximum in the STD profiles (i.e the maximum size of the  
332 agglomerates), as a function of binder flow rate. The evidence that when flow rate increases, the  
333 maximum granule size is reached with larger amount of liquid binder, suggests that a competition  
334 between liquid addition rate and liquid adsorption rate (by the MCC primary particles) exists. The  
335 second evidence that the size of the wet agglomerates starts to reduce before the liquid binder  
336 addition is stopped, suggests that also a competition between growth and breakage mechanisms  
337 exists. Since MCC particles are porous, the capillaries within the porous particles draw liquid into  
338 the interior of the particle, leaving at the surface less liquid available to form bridge bonds with  
339 other particles. If a sufficient fluid flow rate is used to saturate the MCC particles, or at least allow  
340 them to become surface wet, new MCC particles can be continuously incorporated into the  
341 granules. If however liquid addition rate is low, liquid will be completely absorbed into the MCC  
342 internal pores so that new liquid bridges can not form and the growth of the granules start to be  
343 contrasted by the breakage action of the impeller action already at low  $L/S$  ratios. Size reduction  
344 continues until an equilibrium granule size is reached where the strength of the aggregates equates  
345 the shear stresses generated by the impeller. This is a tentative explanation and the full  
346 understanding of the phenomena just described is beyond the scope of this paper which is focused  
347 on the development of an analytical tool.

348 In order to corroborate the idea that constant values of STD profiles at the end of the  
349 granulation process correspond to the same size of the wet agglomerates, the PSDs of the final dry  
350 granules were measured by sieving and as can be observed in Figure 13 they resulted to overlap,  
351 with  $d_{50} = 680 \pm 50 \mu\text{m}$ . The constant value of the final granule size however is not surprising if we  
352 think that, all the formulation variables (type of powder and liquid binder) and the operating

353 conditions (impeller speed, powder amount, massing time), excepted for the binder flow rate, were  
354 the same in all the experiments.

355 Even though the history of the granules was very different (different residence time in the  
356 batch mixer, different duration of the growth and consolidation phases) the final PSDs were very  
357 similar. This observation in addition to the fact that all the experiments were carried out with the  
358 same impeller speed suggests the idea that experiments were operated in the so called mechanical  
359 dispersion regime (Hapgood et al., 2003). In the mechanical dispersion regime the final PSD is  
360 roughly independent of the liquid dispersion modality and wetting dynamics and depends mainly on  
361 the intensity of the mechanical agitation, that in our case was the same in all the experiments.

362

### 363 **3.5. Effect of binder amount**

364 In order to further validate the TA methodology a set of experiments was also performed by  
365 changing the total amount of liquid binder and keeping constant the binder addition time (12  
366 minutes). Therefore the binder flow rate was changed together with the total amount of binder. With  
367 330 g of binder, the flow rate was the same as in the previous experiments 28 ml/min while for 360  
368 g of binder the flow rate increased to 30 ml/min. It can be observed that despite the very small flow  
369 rate variation a significant difference of liquid binder amount was added to the powder in the two  
370 cases ( $\Delta = 30$  g of liquid binder on 300 g of MCC). The corresponding STD profiles are shown in  
371 Figure 14 where it can be observed that:

- 372 • the slope of the STD profiles is roughly constant (linear increase) up to minute 11  
373 independently of the flow rate;
- 374 • large variability of STD profiles can be observed around minutes 12-13;
- 375 • clear differences of the STD profiles can be observed (after stopping liquid addition, i.e.  
376 during massing time) as a function of the total liquid binder amount;

377 It is clear from the Figure that a variation of binder flow rate as small as 2 ml/min in the early stages

378 of the process can not be detected by the TA so that an overlap of the profiles was observed. The  
379 effect of the total binder amount on the final values of STD (end point of granulation) however was  
380 much larger so that significant size differences of the wet agglomerates were observed in the two  
381 cases. Again this observation was corroborated by the measurement of the final PSD (Figure 15).  
382 With 330 g of binder the granule  $d_{50}$  was  $680 \pm 50 \mu\text{m}$ , while for 360 g of binder the  $d_{50}$  was  
383 significantly higher  $1615 \pm 115 \mu\text{m}$ .

384 It has to be noted also that due to the different binder amount also the general trends of the  
385 STD profiles were slightly different. For lower binder amount (330 g) a clear maximum was always  
386 reached, followed by the decrease in size of the agglomerates (as already discussed). For the larger  
387 binder amount (360 g) instead the existence of a maximum in the STD was less evident and  
388 (because of the larger variability of the method in this phase of the process as reported in Figure 9)  
389 it was difficult to draw conclusions on the maximum size reached by the wet agglomerates in this  
390 stage of the process. It can be observed however that for larger binder amount the size reduction  
391 stage is nearly missing, which is physically coherent with the fact that an increased amount of  
392 liquid, added in the same time interval, can generate a larger number of capillary bridges and  
393 increase the strength of the agglomerates.

394

#### 395 **4. Conclusions**

396 An analytical tool based on texture analysis was developed in order to follow the wet  
397 granulation process in a planetary mixer from the beginning up to the end point. Images of the  
398 powder surface within the mixer were captured during the granulation process and analyzed with  
399 several texture indexes. The standard deviation of their gray-scale histogram was selected to  
400 monitor the size evolution of the wet aggregates. The method was critically analyzed showing its  
401 applicability in granulation kinetic studies and in the investigation of the effects of formulation  
402 variables (here reduced for sake of simplicity to the liquid binder amount only). Texture analysis

403 proved to have the ability to give an insight into several aspects of the granulation processes which  
404 of course need to be fully addressed in future contributions.

405

## 406 5. References

407 Bier, H. P., Leuenberger, H., Sucker, H., 1979. Determination of the uncritical quantity of  
408 granulating liquid by power measurements on planetary mixers. *Pharm. Ind.* 41, 375–380.

409 Boerefijn, R., Juvin, P. Y., Garzon, P., 2009. A narrow size distribution on a high shear mixer  
410 by applying a flux number approach. *Powder Technology* 189 (2), 172–176.

411 Briens, L., Daniher, D., Tallevi, A., 2007. Monitoring high-shear granulation using sound  
412 and vibration measurements. *International Journal of Pharmaceutics* 331, 54–60.

413 Cavinato, M., Andreato, E., Bresciani, M., Pignatone, I., Bellazzi, G., Franceschinis, E.,  
414 Realdon, N., Canu, P., Santomaso, A. C., 2011. Combining formulation and process aspects for  
415 optimizing the high-shear wet granulation of common drugs. *International Journal of*  
416 *Pharmaceutics* 416, 229–241.

417 Cavinato, M., Artoni, R., Bresciani, M., Canu, P., Santomaso, A. C., 2013. Scale-up effects  
418 on flow patterns in the high shear mixing of cohesive powders. *Chemical Engineering Science* 102  
419 (0), 1–9.

420 Cavinato, M., Bresciani, M., Machin, M., Bellazzi, G., Canu, P., Santomaso, A. C., 2010.  
421 Formulation design for optimal high-shear wet granulation using on-line torque measurements.  
422 *International Journal of Pharmaceutics* 387, 48–55.

423 Chirkot, T., Propst, C., 1997. Low shear granulators in Handbook of Pharmaceutical  
424 Granulation Technology. Marcel Dekker, New York, 1997, 205-225.

425 Dal Grande, F., Santomaso, A. C., Canu, P., 2008. Improving local composition  
426 measurements of binary mixtures by image analysis. *Powder Technology* 187(3), 205–213.

427 Ennis, B. J., 2006. Theory of granulation: an engineering perspective, in Parikh, D.M.

428 (Ed.), Handbook of Pharmaceutical Granulation Technology, 2nd ed. Taylor and Francis Group,  
429 New York (U.S.A.), pp. 7-78.

430 Faure, A., York, P., Rowe, R., 2001. Process control and scale-up of pharmaceutical wet  
431 granulation processes: a review. *European Journal of Pharmaceutics and Biopharmaceutics* 52,  
432 269–277.

433 Gonzales, R. C., Woods, R. E., Eddins, S. L., 2004. Digital Imaging Processing using  
434 Matlab. Pearson Prentice-Hall.

435 Ryan Gosselin, R., Duchesne, C., Rodrigue, D., 2008, On the characterization of polymer  
436 powders mixing dynamics by texture analysis, *Powder Technology* 183, 177-188.

437 Hapgood, K. P., Iveson, S. M., Litster, J. D., Liu, L. X., 2007, Granulation rate processes, in  
438 Salman, A.D., Hounslow, M.J., Seville, J.P.K. (Eds.) Granulation. Elsevier B.V., pp. 898–977.

439 Hapgood, K. P., Litster, J. D., Smith, R., 2003. Nucleation regime map for liquid bound  
440 granules. *AIChE J.* 49, 350–361.

441 Harnby, N., 1997. Mixing in the process industries. Butterworth-Heinemann, Oxford, UK.

442 Hiseman, M. J. P., Laurent, B. F. C., Bridgwater, J., Wilson, D. I., Parker, D. J., North, N.,  
443 Merrifield, D. R., 2002. Granular flow in a planetary mixer. *Chemical Engineering Research and*  
444 *Design* 80 (5), 432–440.

445 Huang, J., Kaul, G., Utz, J., Hernandez, P., Wong, V., Bradley, D., Nagi, A., O’Grady, D.,  
446 2010. A practical approach to improve process understanding of high shear wet granulation through in-  
447 line particle measurement using fbrm c35. *Journal of Pharmaceutical Sciences* 99(7), 3205–3212.

448 Knight, P. C., Seville, J. P. K., Wellm, A. B., Instone, T., 2001. Prediction of impeller torque  
449 in high shear powder mixers. *Chemical Engineering Science* 56, 4457–4471.

450 Laitinen, N., Antikainen, O., Yliruusi, J., 2002. Does a powder surface contain all necessary  
451 information for particle size distribution analysis? *European Journal of Pharmaceutical Sciences*  
452 17, 217–227.

453 Lakio, S., Hatara, J., Tervakangas, H., Sandler, N., 2012. Determination of segregation  
454 tendency of granules using surface imaging. *Journal of Pharmaceutical Sciences* 101 (6), 2229–  
455 2238.

456 Laurent, B. F. C., 2005. Structure of powder flow in a planetary mixer during wet-mass  
457 granulation. *Chemical Engineering Science* 60 (14), 3805–3816.

458 Leuenberger, H., Puchkov, M., Krausbauer, E., Betz, G., 2009. Manufacturing  
459 pharmaceutical granules: Is the granulation end-point a myth? *Powder Technology* 189, 141–148.

460 Litster, J. D., Ennis, B., 2004. The science and engineering of granulation processes. Kluwer  
461 Powder Technology Series.

462 Middlemann, S., 1995. Modeling axisymmetric flows: dynamics of films, jets, and drops.  
463 Academic Press, Inc.

464 Paul, E. L., Atiemo-Obeng, V. A., Kresta, S. M. (Eds.), 2003. Handbook of Industrial  
465 Mixing: Science and Practice. Wiley-Interscience, John Wiley & Sons, Inc., Hoboken, New Jersey.

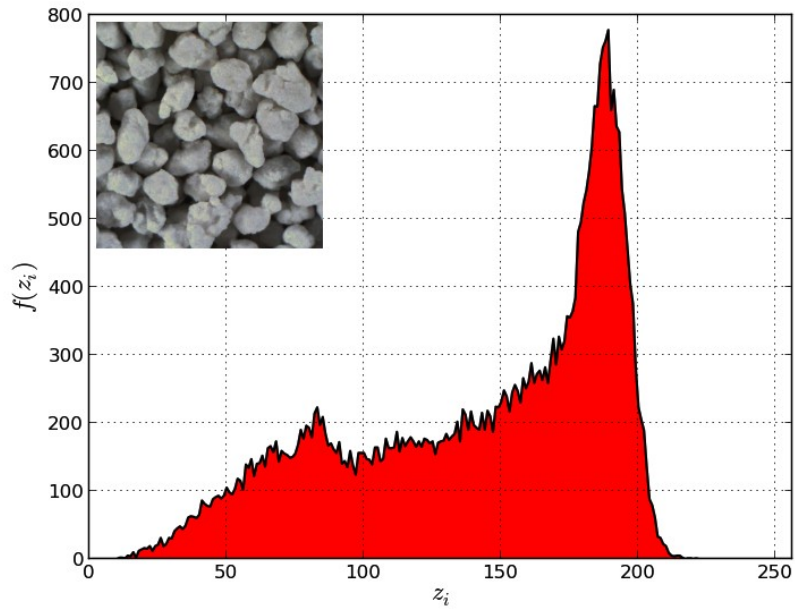
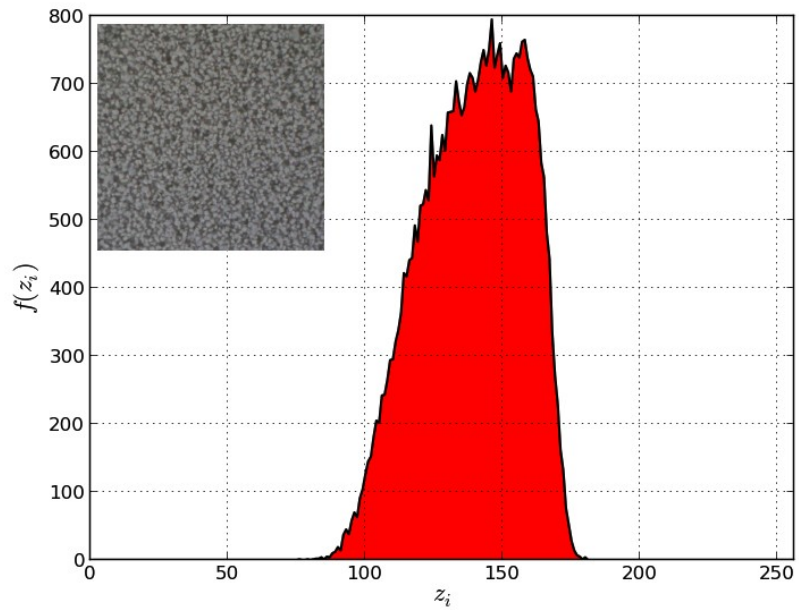
466 Russ, J., 1999. The Image Processing Handbook, 3rd Edition. Boca Raton, FL: CRC Press.

467 Tok, A. T., Goh, X., Ng, W. K., H., T. R. B., 2008. Monitoring granulation rate processes  
468 using three pat tools in a pilot-scale fluidized bed. *AAPS PharmSciTech* 9 (4), 1083–1091.

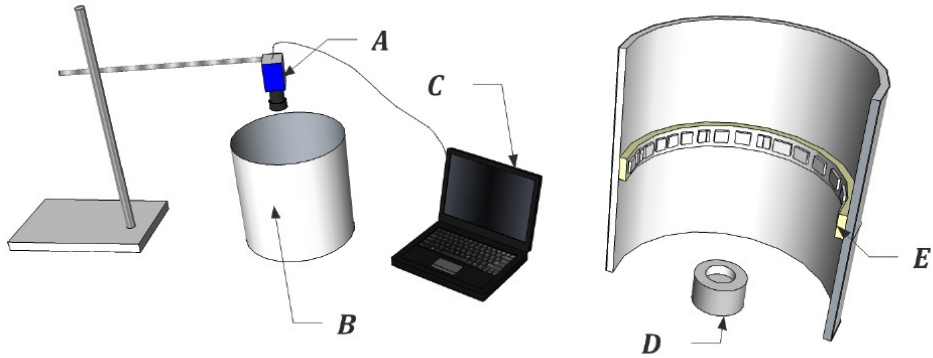
469 Watano, S., 2001. Direct control of wet granulation processes by image processing system.  
470 *Powder Technology* 117, 163–172.

471 Watano, S., 2007. Online monitoring, in Salman, A.D., Hounslow, M.J., Seville, J.P.K. (Eds.)  
472 Granulation. Elsevier B.V., pp. 478–498.

473 Watano, S., Numa, T., Miyanami, K., Osako, Y., 2001. A fuzzy control system of high shear  
474 granulation using image processing. *Powder Technology* 115, 124–130.



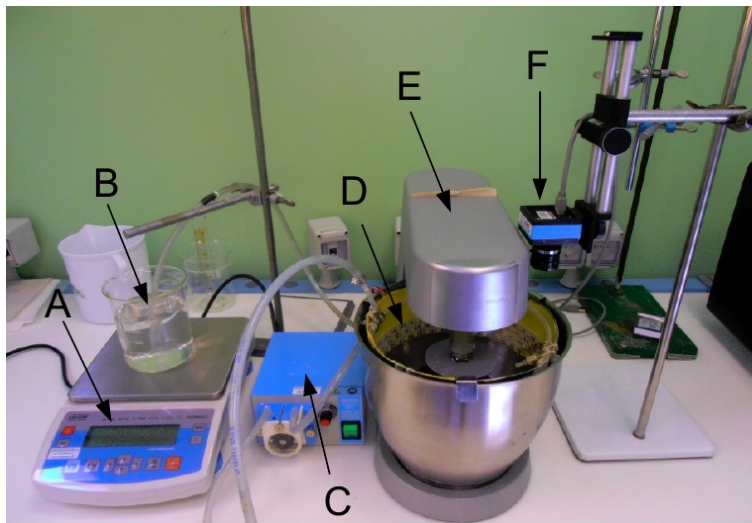
479 **Figure 1:** Example of histograms of intensity levels for two different particle sizes.



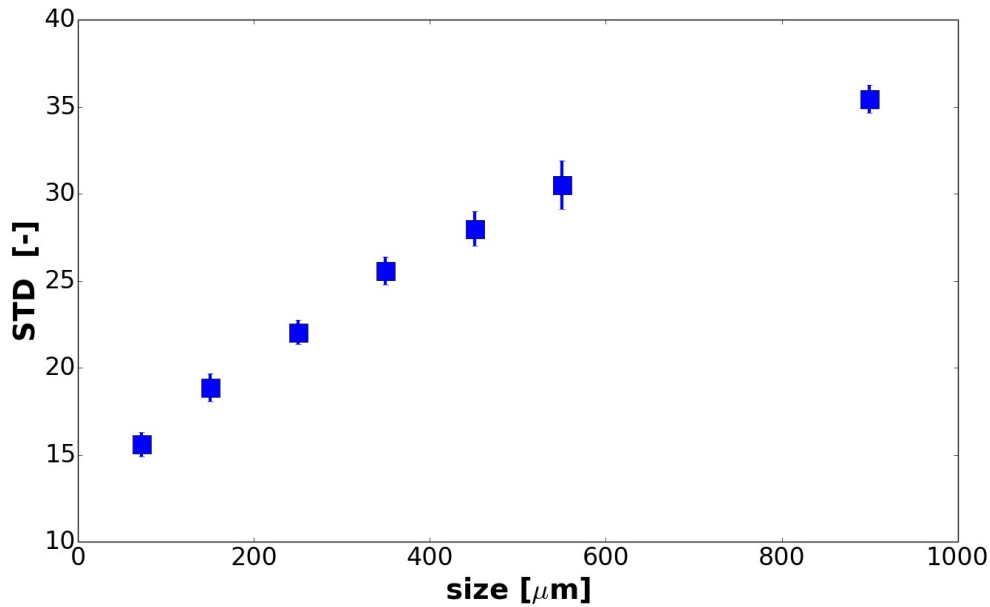
481 **Figure 2:** Experimental set-up for taking images from static samples. A) Digital camera. B)  
 482 Photographic box containing the sample of powder protected from external light. C) Computer for  
 483 image storage. D) Sample holder. E) The photographic box is represented magnified and sectioned  
 484 to show the position of the sample holder and of the ring of LEDs.

485

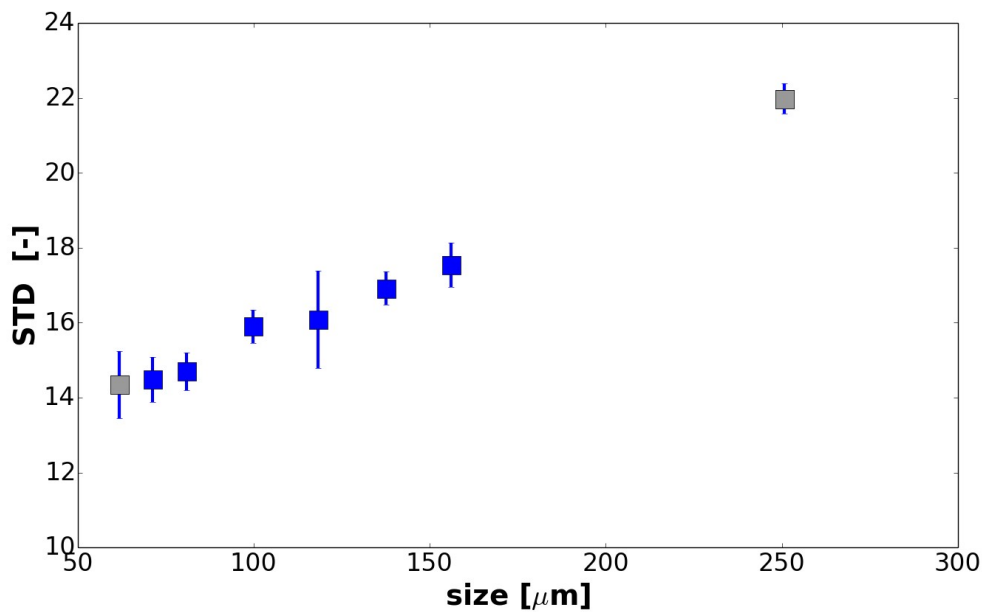
486



487 **Figure 3:** Experimental set-up for dynamic analysis of the granulation process. A) Electronic  
 488 balance. B) Liquid binder dispersion. C) Peristaltic pump. D) Metallic circular structure holding  
 489 three rings of LEDs for even illumination of the powder bed surface. E) Planetary mixer. F) Digital  
 490 camera, connected to a frame grabber and a personal computer (not shown).



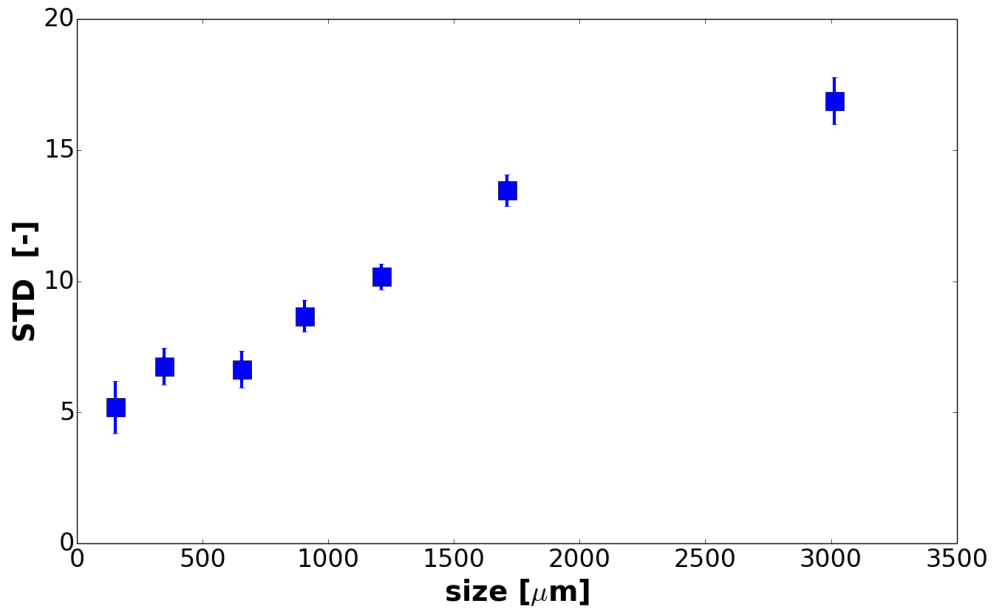
491 **Figure 4:** STD of the gray-scale histogram of the powder bed surface as a function of particle size  
 492 (monodispersed samples).



493 **Figure 5:** STD of the grey scale histogram of binary mixtures of MCC powder and granules as a  
 494 function of the average particle size (bidispersed samples). Eight mixtures were analysed (0, 0.1,  
 495 0.2, 0.4, 0.5, 0.6, 0.8, 1.0 w/w). The two grey point refers to pure MCC powder and to pure  
 496 granules.

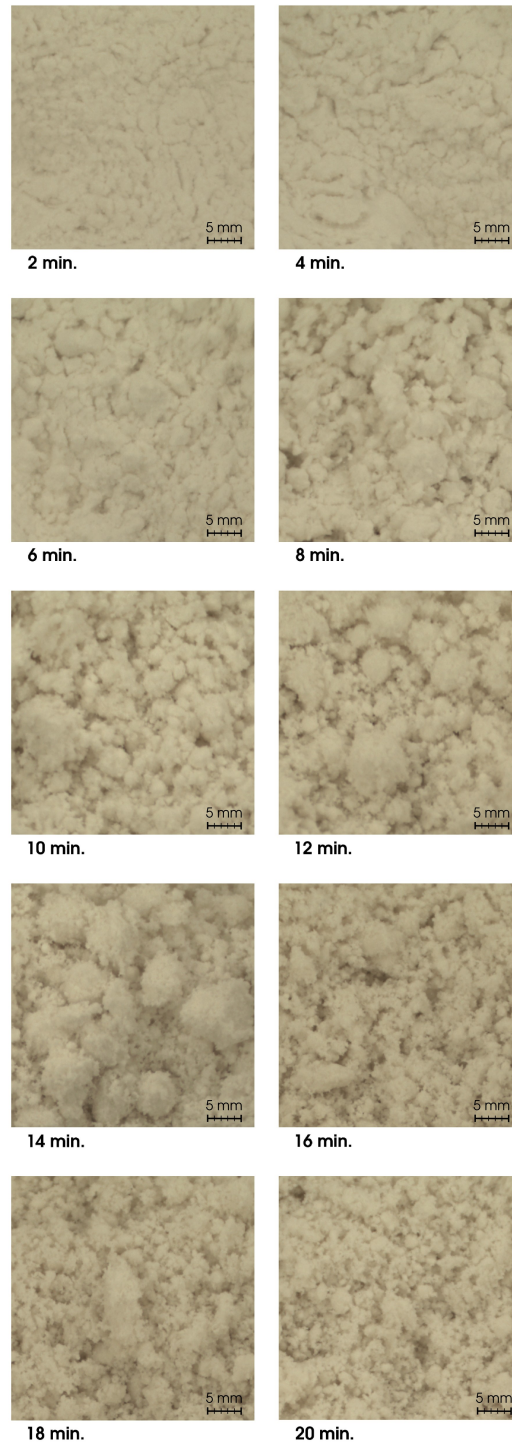
497

498

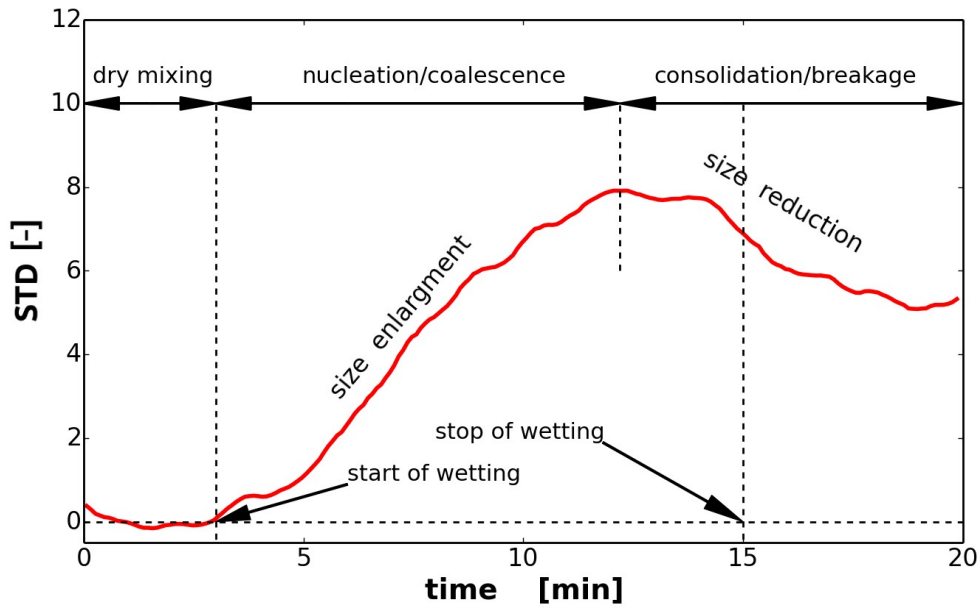


499 **Figure 6:** Dynamic analysis of the surface. STD of the gray-scale histogram as a function of the  
500 size.

501

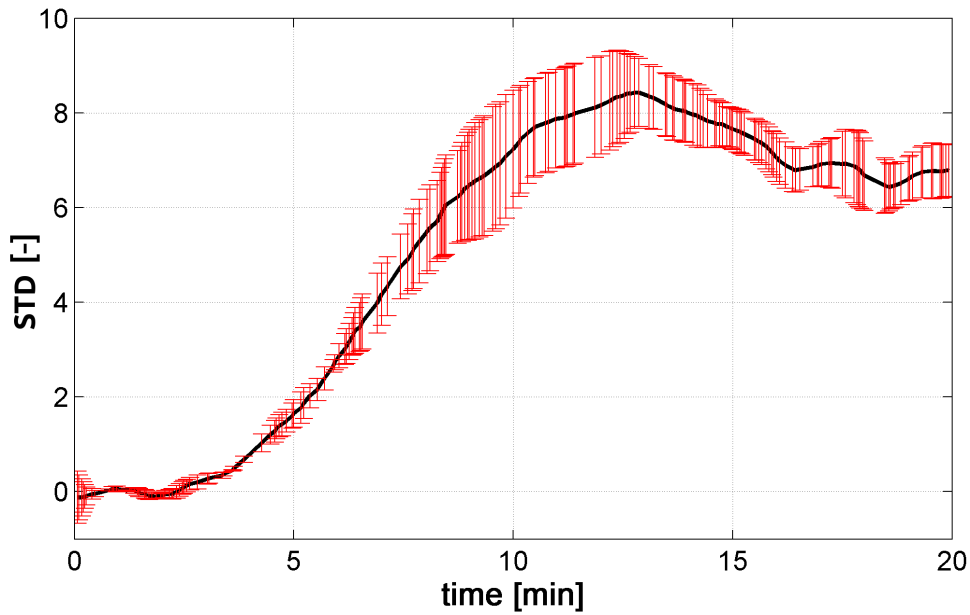


502 **Figure 7:** Evolution of the bed surface texture as a function of binder addition. The experiment was  
503 carried out at the following conditions: binder composition: 0.05% XG; binder addition rate: 28  
504 ml/min; water amount: 330g.



506 **Figure 8:** Typical profile of STD as a function of time during the granulation process.

507

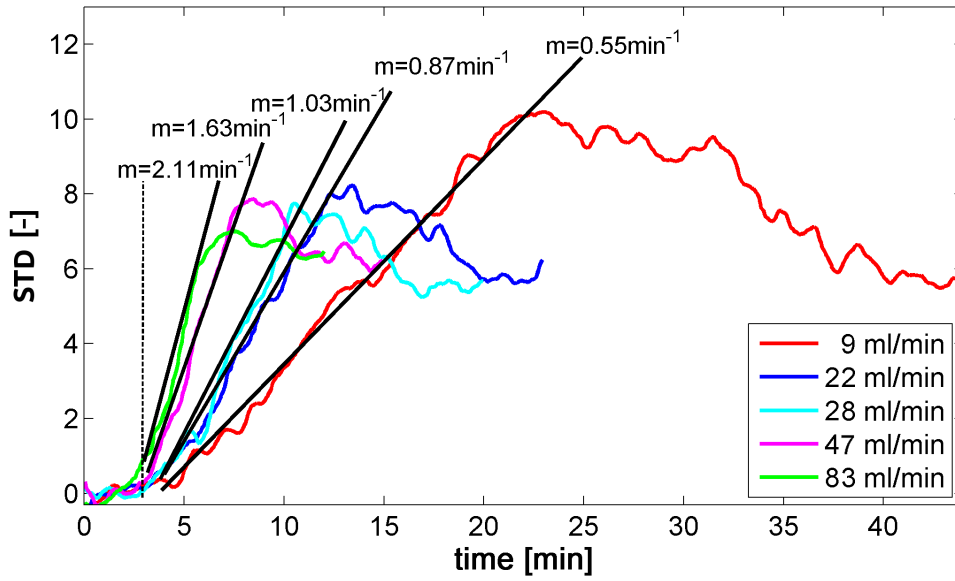


509 **Figure 9:** STD profile showing the typical variability of the granulation process and of the texture  
 510 analysis.

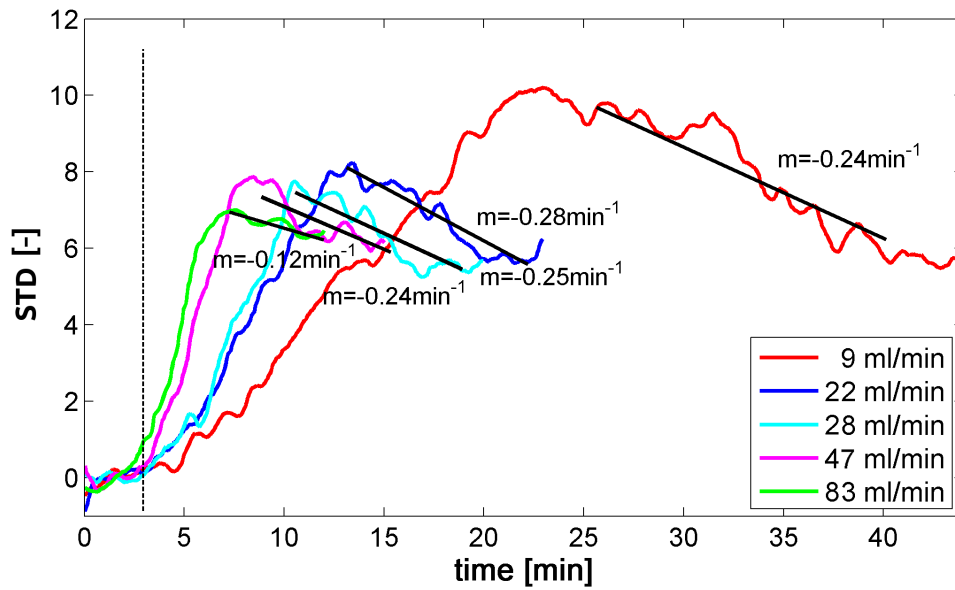
511

512

513 a)

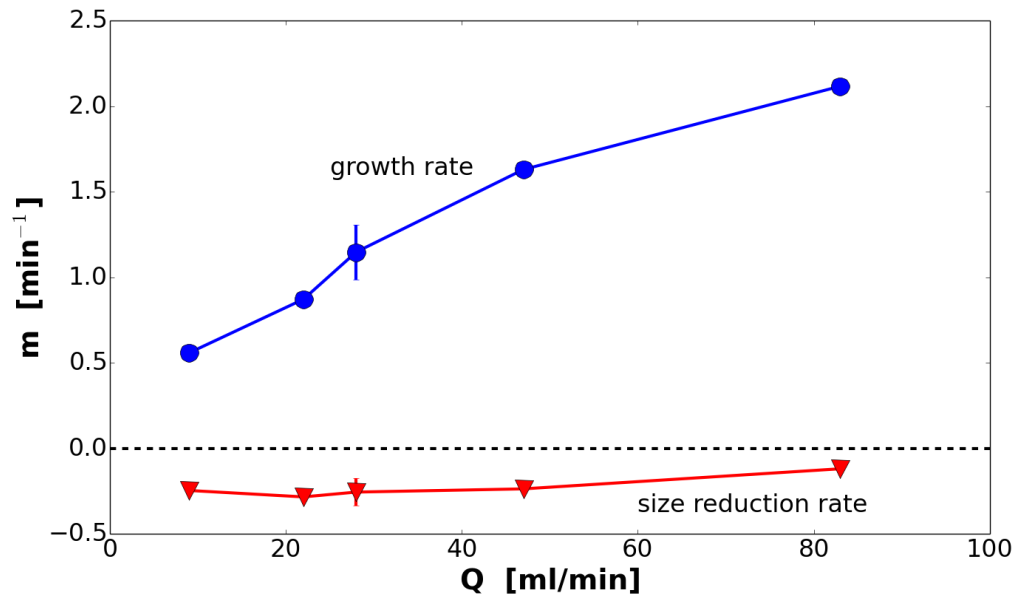


515 b)



517 **Figure 10:** STD profile obtained for XG based binder (0.05 w/w%) at different flow rates and their  
518 linear interpolation in the size enlargement a) and size reduction b) stages.

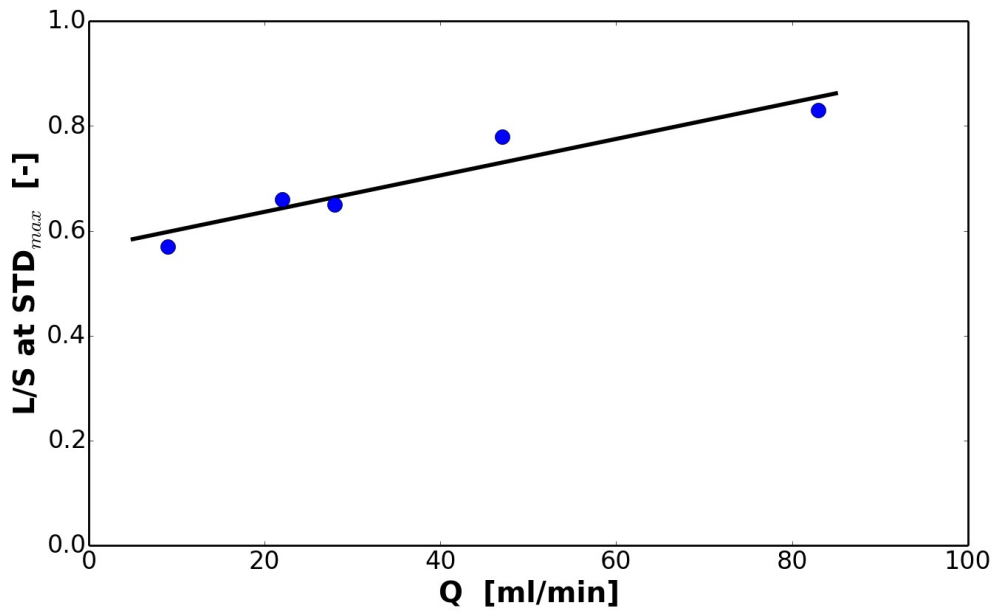
519



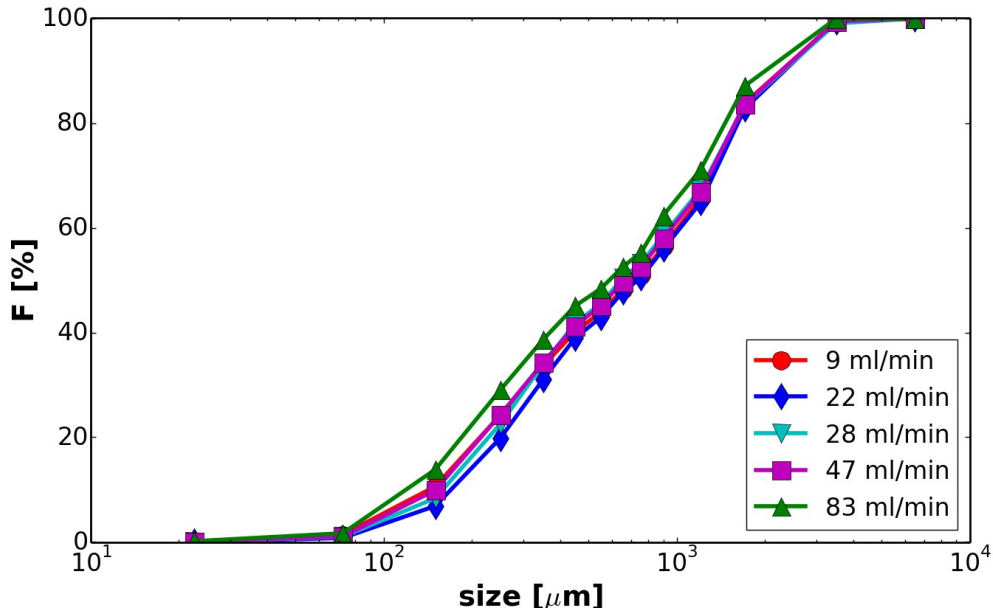
521 **Figure 11:** Kinetic constants  $m$  of the size growth and reduction as a function of the flow rate  $Q$ .

522 Values are obtained from the slopes measured in Figure 10.

523

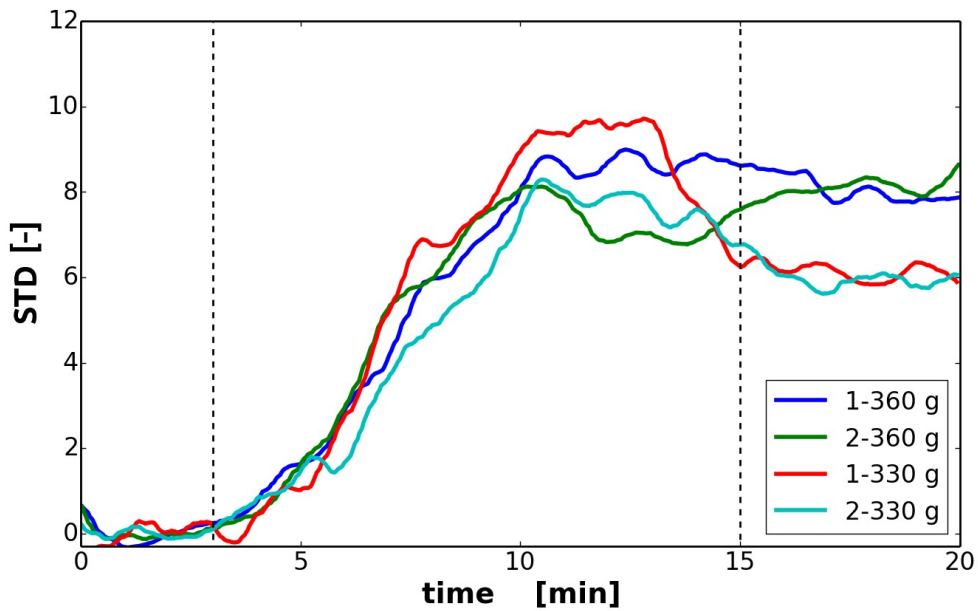


524 **Figure 12:** Liquid to solid ratio at the maximum of STD, as a function of the binder flow rate.

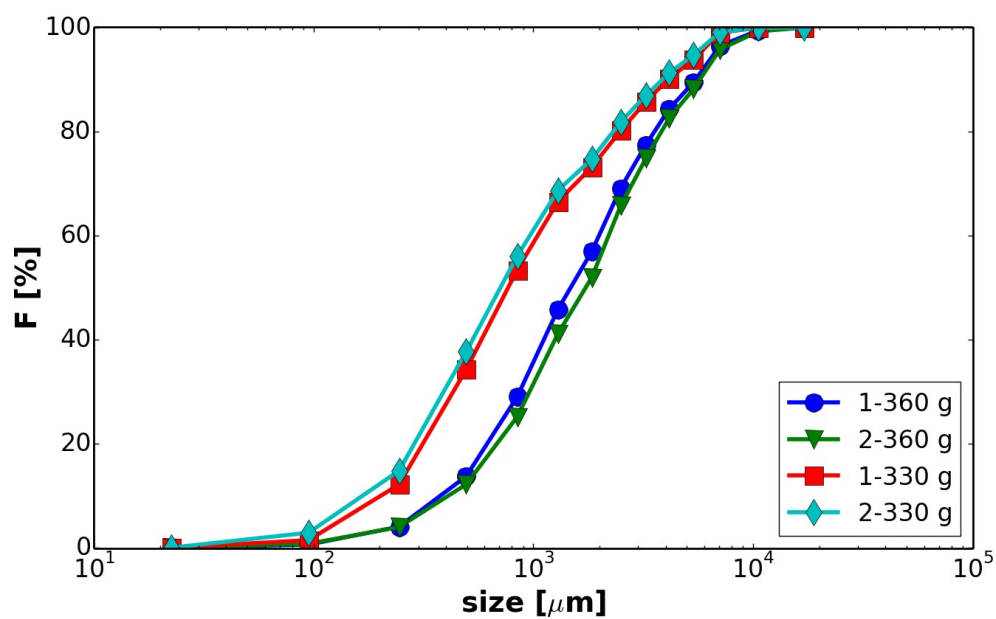


526 **Figure 13:** Cumulative mass fraction of granules obtained with dispersion of XG =0.05% w/w at  
 527 different flow rates.

528



530 **Figure 14:** STD profiles for two different total amount of liquid binder (360 g and 330 g of binder  
 531 respectively). Experiments have been replicated twice.



533 **Figure 15:** Cumulative mass fraction of granules prepared using two different amount of binder.

534 XG=0.05% w/w.